Articles

Three-Dimensional X-ray Microtomography

BRIAN P. FLANNERY, HARRY W. DECKMAN, WAYNE G. ROBERGE, KEVIN L. D'AMICO

The new technique of x-ray microtomography nondestructively generates three-dimensional maps of the x-ray attenuation coefficient inside small samples with approximately 1 percent accuracy and with resolution approaching 1 micrometer. Spatially resolved elemental maps can be produced with synchrotron x-ray sources by scanning samples at energies just above and below characteristic atomic absorption edges. The system consists of a high-resolution imaging x-ray detector and high-speed algorithms for tomographic image reconstruction. The design and operation of the microtomography device are described, and tomographic images that illustrate its performance with both synchrotron and laboratory x-ray sources are presented.

WE HAVE DEVELOPED A NEW FORM OF MICROSCOPY, based on high-resolution x-ray tomography, that produces three-dimensional images of the internal structure of small samples with micrometer resolution. Compared with conventional optical and electron microscopies or the more recently developed nuclear magnetic resonance imaging, acoustic, and scanning tunneling microscopies, x-ray microtomography offers unique imaging capabilities. In particular, accurate three-dimensional maps of density and elemental distributions can be obtained noninvasively. With modern synchrotron x-ray sources, samples can be scanned in less than an hour, a rate competitive with other established microscopies. The technique consists of a high-resolution imaging x-ray detector and high-speed tomographic image reconstruction procedures together with a collimated monochromatic area-filling x-ray beam. When used with an intense synchrotron x-ray source, the method achieves resolution approaching 1 μm and can be conveniently operated to create images at precisely tuned x-ray energies (*1*, *2*). The system also functions with conventional laboratory x-ray sources, although with longer scan times, lower resolution, and a limited set of discrete observational energies.

Tomography is widely used in medical radiology to produce noninvasive, diagnostic, cross-sectional images of bone and tissue structure in human patients. Medical computed tomography (CT) scanners use conventional bremsstrahlung x-ray sources, scintillation crystals, and phototubes as detectors, and high-speed data acquisition and processing to create individual planar maps defined on grids of order 500 by 500 pixels with approximately 1-mm resolution and 1% accuracy in contrast (*3*).

There is no inherent physical limitation preventing the use of x-rays for tomographic imaging with resolution greater than the resolution of medical CT. However, microtomography requires generation and detection of x-rays with high spatial resolution and the storage and processing of substantial amounts of data. Some time ago Grodzins (*1*) pointed out that synchrotron sources could, in principle, be used to generate data suitable for tomographic imaging with micrometer resolution. At that time accurate, efficient x-ray detector systems that could be used for high-resolution tomography did not exist. One aspect of our work concerns the development of a digital imaging x-ray detector system capable of submicrometer resolution (*4*). Because the detector records two-dimensional images, it makes efficient use of the area-filling collimated x-ray beam to record data simultaneously in multiple stacked planes suitable for reconstruction of three-dimensional images. Another obstacle associated with microscopic three-dimensional imaging is the amount of data required to map a representative section of a particular sample. Although medical procedures typically produce maps in a few contiguous planes (each containing $\sim 10^6$ elements) that resolve features of interest in a human patient, maps of even a millimeter-sized object with micrometer resolution require 10^9 volume elements for a complete three-dimensional image. We have created tomographic reconstruction procedures that make it possible to analyze tomographic data hundreds of times more rapidly than is possible with conventional filtered back-projection methods (*5*).

Principles of Transmission Tomography

Mathematical analysis shows that a function can be reconstructed from values of its line integrals (*6–8*). Transmission tomography implements the mathematics to create nondestructive cross-sectional images of the internal structure of a sample from measurement and analysis of penetrating radiation directed through the sample in

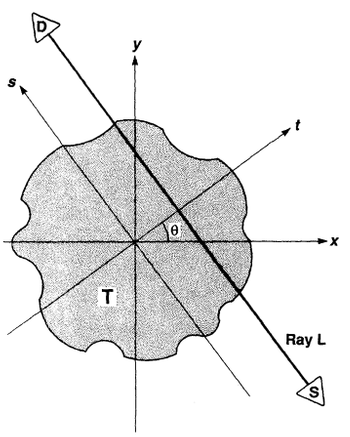

Fig. 1. Coordinate systems used to label positions and observations in a planar section of target T. Ray L indicates a particular measurement between source S and detector D along a path oriented at view angle θ and impact parameter t with respect to Cartesian coordinates (x, y) fixed in the target.

B. P. Flannery, H. D. Deckman, and K. L. D'Amico are at Exxon Research and Engineering Company, Corporate Research Laboratories, Annandale, NJ 08801. W. G. Roberge is assistant professor of physics, Rensselaer Polytechnic Institute, Troy, NY 12180.

multiple coplanar rays (*9*). Along a ray defined by its direction θ and impact parameter t with respect to Cartesian coordinates (x,y) in the observed plane of the sample, the incident (I_0) and transmitted (I_T) intensities of an x-ray beam are related by

$$P(\theta,t) = \ln (I_0/I_T) = \int_s F(x,y)ds \quad (1)$$

where $F(x,y)$ is the linear attenuation coefficient (in cm^{-1}), and s is path length along the ray (Fig. 1). The function $P(\theta,t)$, referred to as a projection measurement or optical depth of the sample along the ray, is the value of the line integral of the attenuation coefficient along the observed ray. One version (*10*) of the mathematical reconstruction formula, the projection-slice theorem, shows that Fourier transform of the target, $\hat{F}(u,v)$, along a ray or slice in frequency space at an angle θ, is identical to the Fourier transform of the projections of the target, $\hat{P}(\theta,\nu)$, viewed from that angle,

$$\hat{F}(u,v) = \iint F(x,y)e^{-2\pi i(ux+vy)}dxdy \quad (2)$$

$$\hat{P}(\theta,\nu) = \int P(\theta,t)e^{-2\pi i\nu t}dt = \hat{F}(u = \nu\cos\theta,\ v = \nu\sin\theta)$$

where u, v, and ν are the transform conjugate variables of x, y, and t, respectively. Thus, in theory, it is possible to generate a map of the attenuation coefficient $F(x,y)$ from measurements of the projections $P(\theta,t)$.

In practical devices, however, the beam may not be attenuated as simply as the idealized law in Eq. 1, and the discrete, imprecise data may not produce an accurate image. For example, the x-ray beam in medical CT devices contains a broad range of energies that attenuate by different amounts so that $F(x,y)$ represents some complex average attenuation integrated over energy and local directionally dependent intensity profiles. Because most materials attenuate x-rays more strongly at lower energy than at higher energy, this effect is known as beam hardening. Also, in most devices, the beam illuminates the sample along many closely spaced paths simultaneously, so that scattering can alter the intensity. Most importantly, the inversion formula, Eq. 2, applies to an infinite set of precise values for the projections. Practical devices acquire a finite amount of data with limited precision. To image a target in which $F(x,y)$ is a band-limited function, that is $\hat{F}(|\nu|) < 0$ for $|\nu| \geq \nu_c$, where ν_c is the cutoff frequency, projection data must be acquired at intervals of impact parameter Δt such that $2\nu_c\Delta t \leq 1$ (*10*). Strictly speaking, a target of finite diameter cannot be band-limited. However, it is reasonable to assume that the projection measurements are band-limited according to the finite resolution of the detector.

Resolution and accuracy of the resultant image depend on the accuracy of the measurements, the geometrical organization of the set of projection data, and the technique used to reconstruct the image. Consider a planar section of a target to be mapped on a Cartesian grid of K^2 pixels, equally spaced at intervals Δx, where the diameter of the target $D \leq K\Delta x$. For an arbitrary target such a map requires observations along at least K^2 independent coplanar paths. There is no unique prescription for data acquisition in tomography. A variety of illumination patterns produce acceptable images, but it is essential to obtain projection data at accurately known positions that match the desired resolution. Figure 2 compares the observational geometry used in conventional medical scanners and our microtomography system. Medical scanners use detectors mounted on a large rim, together with a rotating source that irradiates the target in a fixed fan of $\sim K$ rays from a set of $\sim K$ view angles $0 \leq \theta \leq 2\pi$. Our microtomography device acquires projection data along N plane-parallel impact parameters, spaced at equal intervals Δt, from each of M view angles $0 \leq \theta < \pi$, equally spaced at intervals $M\Delta\theta = \pi$. This geometrical pattern provides adequate resolution to reconstruct $F(x,y)$ if $2\nu_c\Delta t < 1$, and $D\Delta\theta \leq 2\Delta t$, that is, if $M \geq \pi N/2$. For observations matched to the pixel spacing in the reconstruction, $\Delta x \approx \Delta t$, or $K \approx N$. Of course, the image can be reconstructed on a grid of $K < N$ pixels, with less resolution but higher accuracy.

In addition, by using a collimated beam of large size compared with the sample, and by using a panoramic detector, the microtomography system acquires data simultaneously in a large number of stacked coplanar sections. Thus, the data from one set of M two-dimensional projection measurements allow us to reconstruct several hundred sequential planes of the sample to form a three-dimensional map.

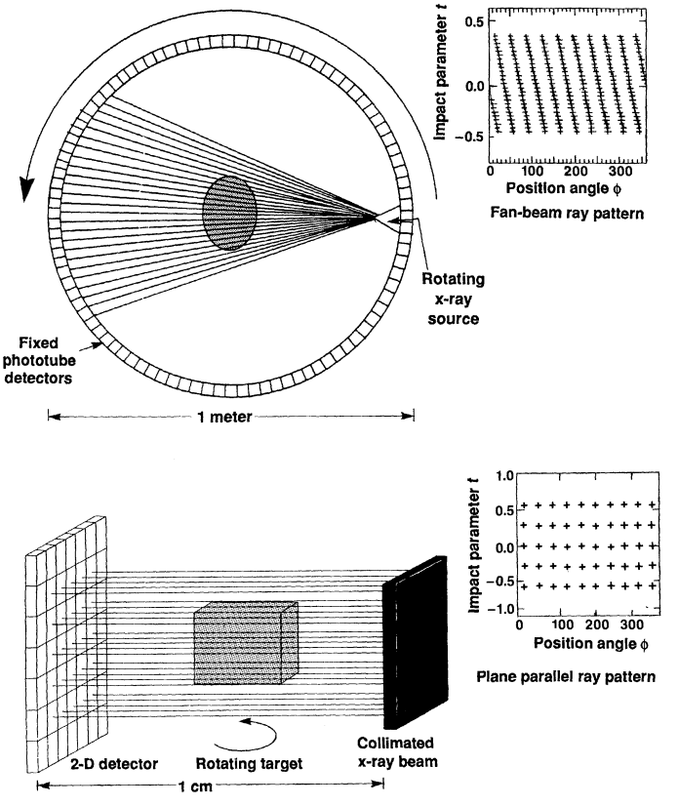

Fig. 2. A schematic comparison of the source-detector configuration in conventional medical CT scanners (**top**) and the x-ray microtomography device (**bottom**). Note that the set of projection measurements occurs in a fan-beam pattern with the medical scanner, and in a plane-parallel pattern in the microtomography system. The medical scanner acquires data in a single plane by rotating the source along the rim containing detectors. The microtomography configuration uses a fixed source producing a large beam of collimated radiation and a panoramic detector to record data simultaneously in multiple stacked planes from which a complete three-dimensional image can be reconstructed. Insets show distribution of impact parameters for each configuration.

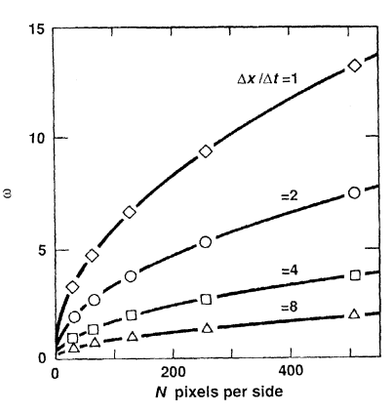

Fig. 3. Noise amplification versus number of projection measurements per view angle. For the observational methodology described in the text, ω represents the ratio of relative uncertainty in the reconstructed image to relative uncertainty in the projection data. Families of curves are labeled by $\Delta x/\Delta t$, the ratio of pixel scale in the image to resolution (detector spacing) in the data. For large N, $\omega \propto N^{1/2}$. Symbols: ◇, $\Delta x/\Delta t = 1$; ○, $\Delta x/\Delta t = 2$; □, $\Delta x/\Delta t = 4$; and △, $\Delta x/\Delta t = 8$.

Conventional single-slice medical CT scanners require extensive computational resources; without more efficient computational methods, three-dimensional tomography would be impractical. Using an array processor (running at ~10 million floating-point operations per second) and a published code (*11*) for filtered backprojection (FBP), the standard tomographic reconstruction algorithm, we found that 2 months of CPU (central processing unit) time would be needed to invert projection data for a three-dimensional sample sectioned into 1000 planar images, each containing maps of 1000 by 1000 pixels. Thus, without faster algorithms or higher speed computers, tomography in this format would be impractical. Well-known alternate reconstruction methodologies based on direct Fourier inversion (DFI) offer advantages in speed: whereas with FBP the number of arithmetical operations required to reconstruct an N by N image scales as N^3, with DFI the number increases only as N^2 ($\log_2 N$ + constant). However, until now, DFI methods have been unsuccessful in producing satisfactory tomographic reconstructions of complex targets. Roberge and Flannery (*5*) describe an improved implementation of DFI that incorporates high-order interpolation methods and filtering in the Fourier domain, which, compared with FBP, produces images of equal quality, but with dramatic improvement in speed. For example, CPU time (on the array processor cited above) to reconstruct 1000 images of 1000 by 1000 pixels each, decreases by a factor of ~200 from 2 months to ~8 hours. Additional computer time is required to read, sort, correct, and calibrate raw data, but these operations do not require such extensive CPU utilization as does image reconstruction. Overall, three-dimensional tomographic imaging requires substantial data processing resources in CPU time, memory, and graphical display.

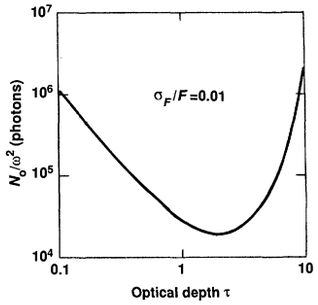

Fig. 4. The number of incident photons required per projection measurement (when Poisson noise is the dominant source of uncertainty) to produce a reconstructed image with relative accuracy $\sigma_F/F = 0.01$; τ is the optical depth of the sample, and the noise amplification factor ω is defined in Eq. 3 and illustrated in Fig. 3. For other values of σ_F/F, $N_0 \propto (\sigma_F/F)^{-1/2}$. Note the minimum in N_0 at $\tau = 2$.

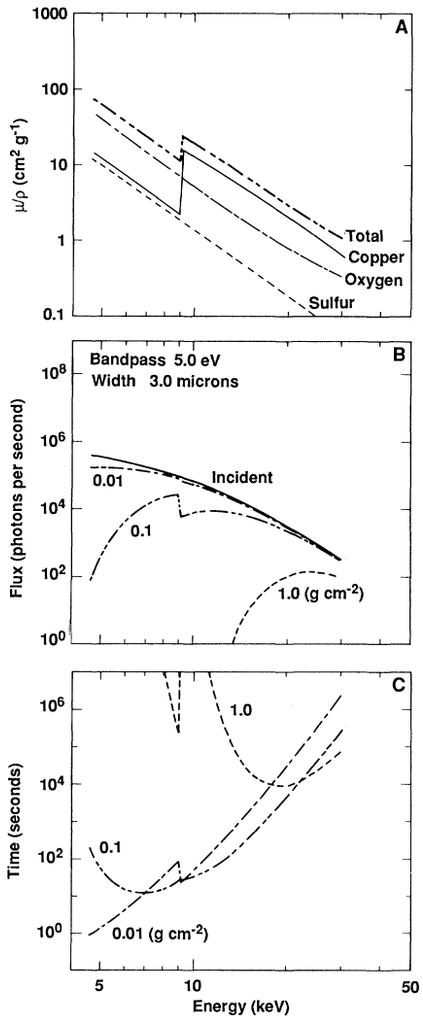

Fig. 5. Variation of (**A**) x-ray attenuation coefficient, (**B**) transmitted intensity, and (**C**) exposure time with x-ray energy, for copper sulfate solution. The Brookhaven NSLS spectrum was used to compute incident intensity and exposure times, under the assumption that 100% of the raw beam could be used on target, and that detectors operate with 100% quantum efficiency. Note the large variation of exposure time with energy and target size.

Accurate tomographic images require precise measurements of beam intensity. Reconstruction procedures amplify noise in the image relative to noise in the projection data by significant factors (*11–13*). Although detailed aspects of the propagation of uncertainty from data to image depend on the exact nature of the target, it is possible to derive relations that capture the principal scaling laws. For the set of plane parallel projection measurements used in the microtomography device, as described above, Roberge and Flannery (*13*) express the noise amplification, ω, as

$$\omega^2 \equiv \left[\frac{\sigma_F/F}{\sigma_P/P}\right]^2 = B\left[\frac{D\Delta t}{\Delta x^2}\right] \tag{3}$$

where σ_F and σ_P are standard deviations in derived and measured values of the attenuation coefficient and projection data, respectively, and B is a numerical coefficient of order unity. Figure 3 illustrates results for the variation of ω. As an example, for image reconstruction on a square grid of $K = D/\Delta x = 256$ pixels per side, with $\Delta t = \Delta x$, $\omega \approx 10$. Consequently, the relative error in projection data must be $\sigma_P/P \leq 0.001$ to reconstruct images with 1% relative accuracy σ_F/F. Note that, for projection data with a given accuracy, noise in the image depends primarily on K, the number of pixels in the image: when $\Delta x \propto \Delta t$, $\omega^2 \propto K$.

If the projection values are determined using photon counting detectors, then Poisson counting statistics provide a minimum estimate of the uncertainty in measured values of P. The number of incident photons required in each projection measurement, N_0, in order to reconstruct the image with specified relative accuracy σ_F/F is

$$N_0 = \frac{\omega^2 \exp(\tau)}{[\tau\ (\sigma_F/F)]^2} \tag{4}$$

where $\tau = \langle FD \rangle$ is the average attenuation through the target (*2*). As pointed out by Grodzins (*1*), notice in Fig. 4 that N_0 exhibits a minimum at $\tau = 2$. For targets of smaller optical depth, the transmitted intensity is higher, which gives a more accurate detected signal, but the measure used in analysis is attenuation, which becomes smaller. For targets of larger optical depth, the transmitted signal decreases exponentially, which gives less accurate data. Also, note that photon counting detectors must accumulate many counts for accurate imaging. For example, to image a planar section of a target of optical depth $\tau = 2$, with 1% accuracy in the reconstruction, on a resolved grid of 256 by 256 pixels requires $N_0 \approx 4 \times 10^6$, in each of $NM \approx 10^5$ directions. For detectors with quantum efficiency $\epsilon < 1$, $N_0 \propto \epsilon^{-1}$.

If Poisson noise dominates measurement uncertainty, the previous results combine to provide two important relations. First, other

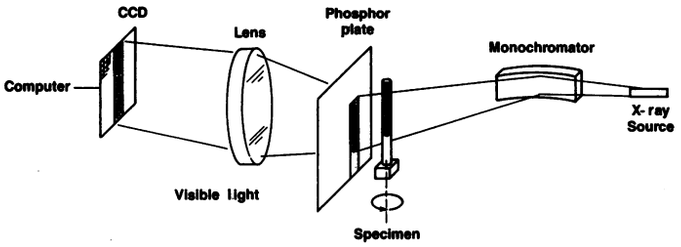

Fig. 6. Schematic of the x-ray microtomography device. A collimated beam of monochromatic x-rays illuminates a sample mounted on a rotatable stage. The intensity of the transmitted x-ray beam is recorded in a digital, panoramic, electro-optic detector. At the heart of the device is a phosphor face plate that converts x-rays to optical radiation with high resolution.

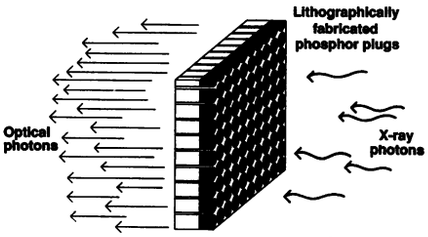

Fig. 7. Schematic of the cellular phosphor plate for conversion of x-rays to optical light. Resolution is limited by the spacing of cells, which can be less than 1 μm. The cells have high quantum efficiency over a broad dynamic range of x-ray intensity. Once converted from x-rays to optical light, the physical scale of the image can be altered with the use of conventional lenses.

factors remaining constant, the accuracy of a reconstructed image scales as $N_0^{1/2}$. Second, to re-image a planar section of a given target with higher resolution Δt, while maintaining equal accuracy, the total dose of x-rays, $NM \times N_0$, needed to create a planar image scales as Δt^{-3}. For a three-dimensional image, dose scales as Δt^{-4}. Thus, dose and exposure time become important considerations when imaging small targets at high resolution.

In microtomography, exposure also depends sensitively on x-ray energy (*1, 2*). To minimize the number of x-rays required in the exposure (*1*), the target should be examined with x-rays at an energy such that $\tau(E) = 2$. If the goal is to minimize observation time (*2*), then characteristics of the source spectrum must also be considered. Synchrotron sources are weaker at higher energy, so minimum exposure time typically requires observations at somewhat lower energy where $\tau \geq 2$. As shown in Fig. 5, the exposure time depends strongly on the size and composition of the target. Finally, in microtomography the ideal observational energy often falls in a range where it is possible to image the sample above and below a characteristic absorption edge of some particular atomic species. By digital image subtraction such observations quantitatively determine the spatial distribution of that element.

Design and Operation of a Microtomography System

As pointed out some time ago by Grodzins (*1*), synchrotron x-ray sources produce an intense, well-collimated beam of x-rays that is ideal for high-resolution tomography. Identical principles govern the use of conventional or synchrotron x-rays in tomography. However, compared with conventional sources, the millionfold enhancement of radiance with synchrotron sources makes it possible to direct an identical number of x-rays through a projected area with a linear scale one thousand times smaller. Thus, resolution can be lowered from ~1 mm to ~1 μm. The ability to tune the energy and bandpass of synchrotron sources offers further potential benefits, as described above. However, until now, there have been no detectors available that can record x-rays accurately and rapidly enough for tomographic applications at such small scales.

At the heart of our device is a novel electro-optic detector that records digital, panoramic x-ray images with ~1 μm resolution and high accuracy over a large dynamic range (*4*). The principal components of the microtomography observational system are shown in Fig. 6. They consist of (i) a source of collimated, preferably monochromatic, x-rays, (ii) a rotatable stage that holds samples, and (iii) the panoramic detector. The novel element in the detector is a lithographically fabricated face plate containing phosphor plugs organized into closely spaced cells (Fig. 7). The cellular phosphor converts x-rays to optical light while maintaining high resolution by confining optical photons within the cells containing the phosphor. Once converted to optical light, the image is magnified with a conventional lens system and focused onto a solid-state, charge-coupled detector (CCD). Aside from the phosphor conversion plate, elements of the detector are commercially available but have been configured to meet the stringent limits required for microtomography.

Resolution of the detector is governed by the optical isolation and spacing of cells in the phosphor plate and the modulation transfer function of the lens system used to relay images from the plate to the CCD. We configured plate and lens combinations which produce resolution of better than 1 μm. Details of the high-resolution, digital, x-ray imaging detector are described elsewhere (*4*). For tomography we have primarily used a phosphor plate with cells spaced apart by ~2.5 μm. When coupled to the CCD with a ×10 microscope objective, we obtain resolution, measured at an edge, of 2.5 μm, or ~1 pixel in the CCD image. This is the expected edge resolution for well-isolated phosphor cells imaged with a lens system that has diffraction-limited resolution significantly smaller than the cell spacing.

Charge-coupled detectors offer attractive properties for microtomography applications. Elements of the detector respond linearly to time-integrated optical intensity over a broad dynamic range of exposure with near zero dark count; the result is a digital image on a two-dimensional array of pixels containing ~10^6 elements. For tomographic measurements the detector must be capable of accurate calibration to better than 1% over a dynamic range of 10^3 in intensity, which is possible with CCDs. However, the inherent physical spacing of active elements on the CCD limits resolution to ~30 μm, and the CCD is unsuitable for long-term direct imaging of x-rays. In combination with the phosphor face plate and magnification of the optical image, the detector achieves an effective resolution of ≤1 μm for panoramic detection of x-rays. In addition, simply by using a larger phosphor conversion plate and suitable optical elements, we can readily image larger targets at lower resolution over an adjustable range of spatial scales up to several centimeters.

To derive projection measurements we must apply several correc-

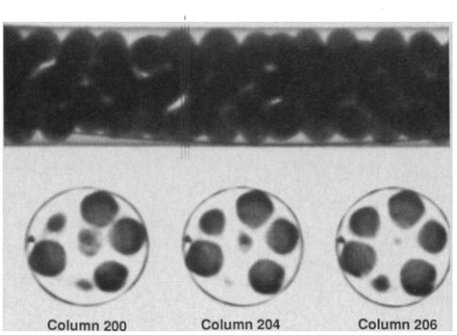

Fig. 8. Calibrated x-ray projection image of a capillary tube (700-μm diameter) packed with silica beads (200-μm diameter) (**top**) and tomographic sections obtained at three consecutive slices indicated in the top figure (**bottom**). Data were obtained with a laboratory x-ray source filtered to operate primarily near 8 keV.

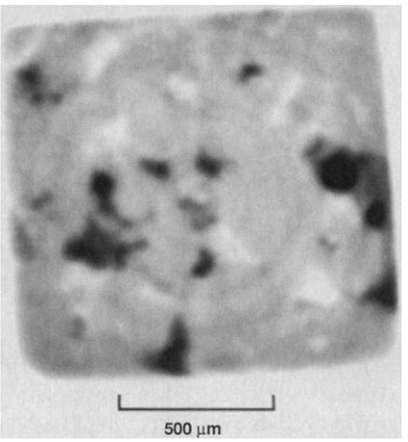

Fig. 9. Tomographic reconstruction of a Coconino sandstone scanned with a laboratory source operating near 8 keV.

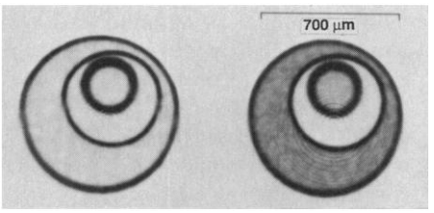

Fig. 10. Tomographic reconstructions of a calibration sample consisting of three nested tubes filled with known concentrations of copper sulfate. The images were obtained with the Brookhaven National Synchrotron Light Source at x-ray energies just above and below the copper K absorption edge.

tion and calibrations steps to the raw CCD data. Individual frames are corrected for pixel-to-pixel variations in gain and zero offset with standard reference procedures to derive correction maps for the CCD. These corrections remain constant for extended periods of time. Also, data must be corrected for signal-dependent background variations attributable to variable scattered light in each image. Obviously, such corrections are most important in highly attenuating samples. Finally, projection values are derived by taking the ratio of an exposure on target to a calibration exposure in which the target is withdrawn from the beam. In practice we acquire a calibration frame every five to ten exposures on target, depending on source stability.

Improper calibration introduces artifacts into the reconstructed image (*14*). To the extent that errors in projection measurements derive from photon counting statistics or other sources of uncorrelated Gaussian noise, the image simply degrades into a mottled appearance on the pixel level, owing to the larger uncertainty (σ_F/F). Persistent, systematic errors introduce more structured artifacts. In particular, calibration errors localized on the detector generate ring-like features in the image. Some such artifacts are evident in the images shown in the next section, but they have been reduced to low amplitude by careful fabrication and calibration procedures.

Principal attributes desired in the radiation source are (i) high intensity levels in a narrow energy range, (ii) nearly parallel collimation, and (iii) beam stability in position and intensity. To achieve resolution Δt in a cross-sectional map of an object of maximum diameter D, penumbral shadowing from the apparent source size and beam divergence cannot exceed an angle $\alpha \approx \Delta t/D$ in passing through the target into the detector. Items (i) and (ii) especially place stringent limits on design because loss of flux usually accompanies high collimation.

Synchrotron sources are ideal for microtomography. At the Exxon X10A beamline at Brookhaven's National Synchrotron Light Source (NSLS) the focused x-ray beam maintains high radiance and collimation over a roughly Gaussian cross-sectional profile ~1 mm in diameter. In addition, the energy can be precisely tuned to illuminate the target in a narrow bandpass ($\delta E/E \approx 6 \times 10^{-4}$) from a broad range of energies (5 keV $< E <$ 15 keV). Thus, it is possible to optimize the observational energy to match the size and composition of a target over a wide range of energy. Exposure times at the NSLS typically are in the range 1 to 10 seconds per view angle, or ≤1 hour for the total data set.

With efficient detectors conventional laboratory x-ray sources provide useful probes for microtomography, but they provide far less flexibility than synchrotron sources because their observational energy cannot be optimized over a continuous range to match the target characteristics. Typically, with laboratory sources, we use filters to isolate a characteristic emission line of the tube. Even with a laboratory scale x-ray source, the microtomography system achieves resolution up to ~100 times higher than conventional CT devices.

For the images shown in the next section the detector was configured with an RCA SID-501 CCD, operated with a controller from Princeton Scientific Instruments, containing approximately 150,000 active pixels organized into 520 rows and 337 columns. The coupled CCD and cellular phosphor produced images at a scale as small as 0.7 μm per pixel. Data for a typical sample reconstructed on a grid of 256 × 256 pixels consists of 400 transmission measurements plus 80 calibration frames with photon counts scaled and recorded with 15-bit encoding. In total a typical data set contains ~10^8 measurements recording a total of ~10^{13} x-ray photons.

Data tapes were processed to reconstruct and display tomographic images. The data processing system involves a combination VAX 11-780 plus Floating Point Systems FPS164 array processor to produce digital images, and an Apollo DN660 imaging graphics computer for display. Images were obtained with the DFI method described by Roberge and Flannery (*5*), which is ideally suited for data acquired in a plane parallel illumination pattern, as in microtomography.

Initial Results for Sample Targets

In this section we illustrate performance of the device by showing images acquired with laboratory and synchrotron x-ray sources.

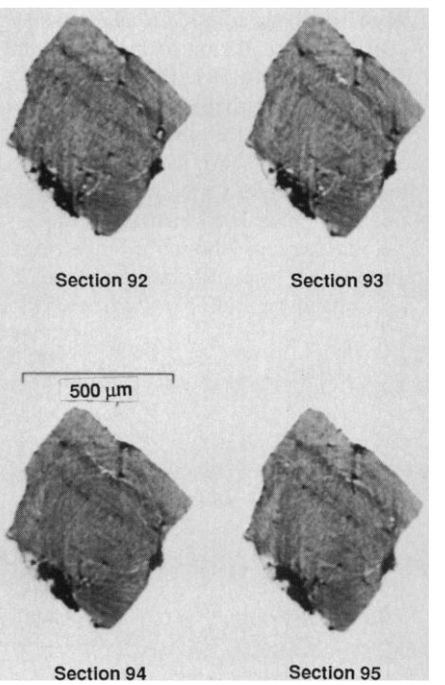

Fig. 11. Tomographic reconstructions of several sequential sections of a half-millimeter-sized sample of Illinois No. 6 coal observed at 6.8 keV with the Brookhaven NSLS with a scale of 2.8 μm per pixel. Roughly horizontal striations across the top of the image appear to represent microscopic bedding planes, whereas dark localized features are regions probably rich in highly attenuating iron.

Figure 8 shows data and tomographic sections from the first sample imaged by means of the microtomography system with a conventional laboratory x-ray source filtered to produce radiation primarily near 8 keV. The top of Fig. 8 shows calibrated projection images of a glass tube 700 μm in diameter filled with silica beads ~200 μm in diameter. From 500 such images, obtained by rotating the tube about its axis, we generated tomographic reconstructions in slices perpendicular to the axis. Three planar slices are shown in the lower half of the figure. Visible in the projection image as a thin line, and in the reconstructions as a dark point, is a tungsten wire 10 μm in diameter that was used to mount the sample.

Figure 9 shows a tomographic reconstruction of an epoxy-impregnated porous rock, a Coconino sandstone, imaged in the laboratory at 8 keV. In this image white areas represent macropores of order 20 to 100 μm in size, the medium tones are primarily SiO_2, and darker areas appear to be material rich in iron. Tomographic images readily distinguish even slight composition differences, because these differences produce measurable changes in the x-ray attenuation coefficient.

Figure 10 illustrates tomographic data acquired at NSLS. The left image is a sample designed to test and calibrate procedures. It is a nested set of thin-walled glass tubes filled with copper sulfate solutions of known concentration. The two images were acquired with x-rays in nearly monochromatic bands of energy just above and below the K edge for absorption by copper. The right image appears darker because attenuation increases strongly above the K edge. Since tomographic analyses work with projection data (optical depth), a dimensionless quantity whose magnitude is determined by the attenuation of the beam, the reconstructed image map directly measures attenuation per pixel. Because the beam is nearly monochromatic, conversion to identifiable physical units only requires knowledge of the physical scale associated with pixel size and the energy of the beam. In this case absolute values for the x-ray attenuation in the tomographic image agree to better than 1% with values predicted from the known composition.

Figure 11 displays four consecutive cross sections from a 0.5-mm sample of Illinois No. 6 coal imaged at 6.8 keV and 2.75 μm per pixel. Image elements in the reconstruction are cubic, so the spacing between planes equals the resolution in the plane (that is, the planar sections are spaced by 2.8 μm). Here the gray scale levels in the image have been adjusted to accentuate the relatively low amplitude variation in attenuation coefficient present in the bulk of the material of the sample. In fact, the three small dark regions of the image contain material that is many times more opaque than the typical coal matrix, but for display purposes all regions more dark than some threshold have been set black. Presumably those highly attenuating regions are rich in iron, known to be present in the sample. A preliminary analysis of the sample suggests that the low-level fluctuations shown in the images possibly are caused by variations in the distribution of sulfur in the bulk coal or by variations in the bulk density of the organic material.

Conclusions

Microtomography can be used to nondestructively generate images of internal sections of a sample with resolution comparable to that of a light microscope. We have illustrated the performance of this technique with results at ~10-μm resolution with a laboratory source and with images at 2.8 μm per pixel obtained at NSLS. It is possible to acquire maps that determine the x-ray attenuation coefficient with ~1% accuracy that can be absolutely calibrated. Thus, microtomography readily distinguishes slight differences in density or composition. By using synchrotron sources to acquire scans at energies just above and below characteristic atomic absorption features, we can selectively map the spatial distribution of elements with accessible absorption edges.

We believe that microtomography will become an important probe and diagnostic tool for investigations in materials science, biology, and medicine. Numerous opportunities exist to improve the capabilities of the technique in terms of resolution, speed of data acquisition, and image format. Similarly, opportunities exist to extend the range of samples that can be scanned by designing improved techniques for sample preparation. Because microtomography is noninvasive, we believe that it will be possible to study contained systems under conditions of temperature, pressure, and environment representative of process conditions in reactors, or biological systems, which cannot be studied with conventional techniques. The synchrotron beam itself produces adequate radiance to allow data acquisition rapidly enough to study some dynamic systems, such as those with flow. Future improvements in computer control and storage devices will make it possible to use real-time microtomography to study dynamic systems. Finally, even with the data collection ability available today, microtomography presents important challenges to design analysis and display capabilities to interpret three-dimensional structural data sets.

REFERENCES AND NOTES

1. L. Grodzins, *Nucl. Instrum. Methods* **206**, 541 (1983).
2. B. P. Flannery and W. G. Roberge, unpublished data.
3. C. C. Jaffe, *Am. Sci.* **70**, 576 (1982).
4. H. W. Deckman, S. Gruner, J. Dunsmuir, unpublished data.
5. W. G. Roberge and B. P. Flannery, unpublished data.
6. J. Radon, *Ber. Verh. Saech. Akad. Wiss. Leipzig, Math. Phys. K1.* **69**, 262 (1917).
7. R. N. Bracewell, *Aust. J. Phys.* **9**, 198 (1956).
8. A. M. Cormack, *J. Appl. Phys.* **34**, 2722 (1963).
9. G. N. Hounsfield, *Br. J. Radiol.* **46**, 1016 (1973).
10. R. M. Mersereau and A. V. Oppenheim, *Proc. IEEE* **62**, 1319 (1974).
11. L. A. Shepp and B. F. Logan, *IEEE Trans. Nucl. Sci.* **21**, 21 (1974).
12. D. A. Chesler, S. J. Reiderer, N. J. Pelc, *J. Comput. Assist. Tomogr.* **1**, 64 (1977).
13. W. G. Roberge and B. P. Flannery, unpublished data.
14. B. P. Flannery, W. G. Roberge, H. W. Deckman, in preparation.

15. We acknowledge the support and contributions of many colleagues at Corporate Research Laboratories of Exxon Research and Engineering who have contributed to various aspects of the microtomography research program, especially P. Eisenberger, R. Hewitt, and D. Moncton, and the staff at Exxon's beamline at NSLS. We also thank J. Dunsmuir, S. Gruner, R. Lee, J. McHenry, and M. Wainger for assistance in the design and operation of the detector system and computer analysis facilities.